


Probing the nature of dark matter via gravitational waves lensed by small dark matter halos

Xiao Guo¹ and Youjun Lu^{1*}

*National Astronomical Observatories, Chinese Academy of Sciences,
20A Datun Road, Beijing 100101, China
and School of Astronomy and Space Science, University of Chinese Academy of Sciences,
19A Yuquan Road, Beijing 100049, China*

 (Received 31 May 2021; revised 3 June 2022; accepted 23 June 2022; published 18 July 2022)

Dark matter (DM) occupies the majority of matter content in the universe and is probably cold (CDM). However, modifications to the standard CDM model may be required by the small-scale observations, and DM may be self-interacting (SIDM) or warm (WDM). Here we show that the diffractive lensing of gravitational waves (GWs) from binary black hole mergers by small halos ($\sim 10^3\text{--}10^6 M_\odot$; minihalos) may serve as a clean probe to the nature of DM, free from the contamination of baryonic processes in the DM studies based on dwarf/satellite galaxies. The expected lensed GW signals and event rates resulting from CDM, WDM, and SIDM models are significantly different from each other, because of the differences in halo density profiles and abundances predicted by these models. We estimate the detection rates of such lensed GW events for a number of current and future GW detectors, such as the Laser Interferometer Gravitational Observatories (LIGO), the Einstein Telescope (ET), the Cosmic Explorer (CE), Gravitational-wave Lunar Observatory for Cosmology (GLOC), the Deci-Hertz Interferometer Gravitational Wave Observatory (DECIGO), and the Big Bang Observer (BBO). We find that GLOC may detect one such event per year assuming the CDM model, DECIGO (BBO) may detect more than several (hundreds of) such events per year, by assuming the CDM, WDM (with mass > 30 keV) or SIDM model, suggesting that the DM nature may be strongly constrained by DECIGO and BBO via the detection of diffractive lensed GW events by minihalos. Other GW detectors are unlikely to detect a significant number of such events within a limited observational time period. However, if the inner slope of the minihalo density profile is sufficiently steeper than the Navarro-Frenk-White profile, e.g., the pseudo-Jaffe profile, one may be able to detect one to more than 100 such GW events by ET and CE.

DOI: [10.1103/PhysRevD.106.023018](https://doi.org/10.1103/PhysRevD.106.023018)

I. INTRODUCTION

The cold dark matter (CDM) model can successfully reproduce the observed large-scale structure, but has difficulties in interpreting small-scale structures [1]. Searches of CDM particles by ground-based experiments have also excluded a large parameter space for weakly interacting massive particles [2], perhaps the most promising CDM candidates [3]. These urge investigations on alternative dark matter (DM) models, such as self-interacting CDM (SIDM) [4], warm DM (WDM) [5], or fuzzy/wavelike DM [6], proposed to generate halos with corelike density profiles and/or smaller abundance at low masses relative to the CDM model.

The abundance and density profile of low-mass halos can be inferred via observations of dwarf/satellite galaxies [7]. However, it may be biased due to the faintness of these galaxies and contamination from not-well understood

baryonic processes [8,9]. Halos with mass $\sim 10^3\text{--}10^6 M_\odot$ (hereafter minihalos), dark and free from complex baryonic processes, are ideal systems to study DM [10], but hard to observe by electromagnetic (EM) waves, even using its gravitational lensing effect [11].

Recently, it was shown that the lensing of gravitational waves (GWs) is an unique method to probe DM halos because the lensing effect leads to detectable waveform changes and resolvable time delays [12–17]. Cao *et al.* [18,19] also proposed that the strong lensing of GWs can be used to probe fluid DM. Not only are a significant number of GW events strongly lensed by galaxies expected to be detected by future GW detectors [20,21], but also GW events diffractively lensed by minihalos may be detectable [12]. Here we show that the gravitational lensing of GWs by minihalos may be used to reveal the nature of DM. We investigate the lensed GW signals caused by minihalos with different density profiles and estimate the event rates of such phenomena by assuming different DM models. The significant differences in the lensed GW signals and event

*luyj@nao.cas.cn

rates resulting from different models clearly demonstrate that the gravitational lensing of GWs can serve as a clean probe to DM nature.

This paper is organized as follows. In Sec. II, we illustrate the diffractive lensing effects on GW signals by minihalos with different mass density profiles. In Sec. III, we introduce the method for identifying the lensing signatures by minihalos, using the SNR difference of the lensed signals from the unlensed ones. In Sec. IV, the detectable lensing rates for stellar binary black hole (sBBH) merger events are estimated by assuming different DM models for the current and future GW detectors. The conclusions are summarized in Sec. V.

II. GW SIGNAL LENSED BY HALOS

Consider a lens system in the wave optics regime: the source (GW event) and lens (DM halo) are locating at redshift z_s and z_ℓ , correspondingly distance D_s and D_ℓ (lens to source $D_{\ell s}$), respectively. The lensed GW signal is

$$\tilde{\phi}^L(f) = F(f)\tilde{\phi}(f) \quad (1)$$

in the frequency domain, where $F(f)$ denotes the factor of (original) unlensed signal $\tilde{\phi}(f)$ amplified by the lens potential. In general, we have

$$F(w, \mathbf{y}) = \frac{w}{2\pi i} \int d^2\mathbf{x} \exp[iwT(\mathbf{x}, \mathbf{y})], \quad (2)$$

where w is a dimensionless frequency (defined later for lenses with different density profiles), $T(\mathbf{x}, \mathbf{y}) = \frac{1}{2}|\mathbf{y} - \mathbf{x}|^2 + \psi(\mathbf{x}) - T_1(\mathbf{y})$, $\mathbf{x} = \frac{\boldsymbol{\xi}}{\xi_0}$ and $\mathbf{y} = \frac{D_\ell}{\xi_0 D_s} \boldsymbol{\eta}$ are dimensionless angular coordinates on the lens and source planes, respectively, $\boldsymbol{\xi}$ the impact parameter, $\boldsymbol{\eta}$ the source position vector, ξ_0 a normalization length, w the dimensionless frequency (defined below for different density profiles), $\psi(\mathbf{x})$ the lens potential (determined by the mass density profile of the lens) [22], and $T_1(\mathbf{y})$ the arrival time of first image under geometrical optics. Obviously diffractive lensing can cause significant frequency-dependent amplification and phase modulation of waveforms [23,23–26]. The calculation of amplification factor can refer to [27].

When $w \rightarrow \infty$, i.e., in the geometrical limit, only stationary points of Fermat potential [or time-delay surface $T(\mathbf{x}, \mathbf{y})$] contribute to the diffraction integral [Eq. (2)]. These stationary points satisfy $\nabla_{\mathbf{x}} T(\mathbf{x}, \mathbf{y}) = 0$, i.e., the lens equation $\mathbf{y} = \mathbf{x} - \nabla_{\mathbf{x}} \psi(\mathbf{x})$. Thus the amplification factor is the summation of multiple images,

$$F_{\text{geo}}(w, \mathbf{y}) = \sum_j \sqrt{|\mu_j|} \exp[iwT_j - i\pi n_j], \quad (3)$$

where $T_j = T(\mathbf{x}_j, \mathbf{y})$ and $\mu_j = \mu(\mathbf{x}_j)$ are for the position and magnification of the j th image \mathbf{x}_j , $n_j = 0, 1/2$, and 1

for the image position at the minimum, saddle, and maximum points of the Fermat potential, respectively (see Refs. [24,28]).

For the spherical symmetrical cases, the lens equation can be reduced to $y = x - d\psi(x)/dx$. By setting $dy(x)/dx = 0$, i.e., $d^2\psi(x)/dx^2 = 1$, we obtain the critical value x_{cr} , thus correspondingly $y_{\text{cr,g}}$, which represents the boundary between cases with single image and double images.

A. Pseudo-Jaffe lens

In the strong lens studies, the pseudo-Jaffe profile is frequently adopted [22], i.e.,

$$\hat{\rho}_{\text{PJ}}(x) = (x^2 + s^2)^{-1}(x^2 + a^2)^{-1}, \quad (4)$$

where s and a ($> s$) represent core and transition radius, respectively [29]. Though small halos may not follow the pseudo-Jaffe profile, we still adopt such a profile for analysis below as reference.

We define $\rho_{\text{PJ}}(x) = \rho_s \hat{\rho}_{\text{PJ}}(x)$, where ρ_s is the scale density and $\rho_{\text{PJ}}(1) = \frac{\rho_s}{(1+s^2)(1+a^2)}$. For convenience, we adopt the scale radius as the same as the Einstein radius of a corresponding singular isothermal sphere (SIS) model with the same ρ_s but with $s \rightarrow 0$ and consider the approximation when $s \ll x \ll a$ (or $a \rightarrow \infty$ but we still keep a in the expression), i.e.,

$$\xi_0 = 4\pi \frac{\sigma_v^2}{c^2} D_{\text{eff}} = 4\pi \frac{\sigma_v^2}{c^2} \frac{D_\ell D_{\ell s}}{D_s}. \quad (5)$$

This scale radius is adopted for convenience though it is not the real Einstein radius of the pseudo-Jaffe lens. The Einstein radius of a pseudo-Jaffe lens can be defined as $y_{\text{cr,g}}\xi_0$, e.g., $y_{\text{cr,g}} \simeq 0.168$ for $(s, a) = (0.1, 2)$; $y_{\text{cr,g}} \simeq 0.637$ for $(s, a) = (0, 2)$.

By analogizing the SIS model, we can substitute σ_v in Eq. (5) with ρ_s ; thus,

$$\xi_0 = \frac{a^2 c^2}{(4\pi)^2 G D_{\text{eff}} \rho_s},$$

since the enclosed mass within radius x is $M(x) = \frac{\sigma_v^2 \xi_0 x}{G}$ for the SIS model. Then the total mass of the pseudo-Jaffe lens and the scale radius are related to each other by $M_\ell = \frac{2\pi^2 \rho_s \xi_0^3}{a+s}$. Finally, we obtain

$$\xi_0^2 = \frac{8(a+s)GM_\ell D_{\text{eff}}}{a^2 c^2}. \quad (6)$$

Therefore, the dimensionless frequency and the time delay in Eq. (2) are

$$w = \frac{2\pi f(1+z_\ell)}{cD_{\text{eff}}} \xi_0^2 = \frac{16\pi f(1+z_\ell)(a+s)GM_\ell}{c^3 a^2},$$

and

$$T = \frac{cD_{\text{eff}}t_d}{\xi_0^2} = \frac{a^2 c^3 t_d}{8(a+s)GM_\ell},$$

where t_d is the real-time delay. The dimensionless mass density for the pseudo-Jaffe profile is

$$\kappa(x) = \frac{\kappa_s}{2} \left[\frac{1}{\sqrt{s^2 + x^2}} - \frac{1}{\sqrt{a^2 + x^2}} \right],$$

where $\kappa_s = \frac{a^2}{2\pi}$. The lens potential can be expressed analytically as

$$\psi(x) = \kappa_s \left[\left(\sqrt{s^2 + x^2} - s \right) - \left(\sqrt{a^2 + x^2} - a \right) - s \ln \frac{s + \sqrt{s^2 + x^2}}{2s} + a \ln \frac{a + \sqrt{a^2 + x^2}}{2a} \right].$$

B. NFW lens and the CDM model

In the CDM model, those DM halos with mass M_ℓ may be actually described by the NFW profile as

$$\rho_{\text{NFW}}(x) = \rho_s x^{-1} (1+x)^{-2}, \quad (7)$$

where ρ_s is the scale density, $x = r/\xi_0$, $\xi_0 = r_s$ the scale radius for NFW profile [30], determined by the halo mass and concentration parameter c_v ($= r_{\text{vir}}/r_s$ and r_{vir} is the virial radius of the halo) as given in [31] (see also Ref. [32]), i.e.,

$$c_v(M_\ell, z_\ell) = \frac{8}{1+z_\ell} \left(\frac{M_\ell}{10^{14} h_0^{-1} M_\odot} \right)^{-0.13}. \quad (8)$$

Here $h_0 = 0.677$ is dimensionless Hubble constant. Adopting the NFW profile, the lens potential is $\psi(x) = \kappa_s \hat{\psi}(x)$, where $\kappa_s \equiv \frac{8\pi G D_{\text{eff}}}{c^2} \rho_s r_s$, a dimensionless parameter, denotes a mass surface density. Different halos have different κ_s but the same $\hat{\psi}(x)$ [33], and low-mass halos have small κ_s . In this case, we can define the typical mass of the lens, the dimensionless frequency, and the time delay as

$$M_{Ez} = \frac{r_s^2 c^2 (1+z_\ell)}{4G D_{\text{eff}}}, \quad (9)$$

$$w = \frac{2\pi f r_s^2 (1+z_\ell)}{D_{\text{eff}} c} = \frac{8\pi G f M_{Ez}}{c^3}, \quad (10)$$

and

$$T = cD_{\text{eff}}t_d/r_s^2. \quad (11)$$

Since r_s is determined by M_ℓ and z_ℓ , M_{Ez} should depend on M_ℓ , z_ℓ , and z_s ; from the above description one can obtain

$$M_{Ez} \propto (r_{\text{vir}}/c_v)^2 \frac{1+z_\ell}{D_{\text{eff}}} \propto M_\ell^{0.927} g_1(z_\ell, z_s), \quad (12)$$

where $g_1(z_\ell, z_s)$ is a function describing the dependence of M_{Ez} on the redshifts of both the GW source and the lens. Similarly, we also have

$$\kappa_s \propto D_{\text{eff}} \rho_s r_s \propto M_\ell^{0.463 + \frac{d \ln \rho_s}{d \ln M_\ell}} g_2(z_\ell, z_s), \quad (13)$$

where $g_2(z_\ell, z_s)$ is a function describing the dependence of κ_s on the redshifts of both the GW source and the lens, and

$$\frac{d \ln \rho_s}{d \ln M_\ell} = \frac{d \ln \rho_{\text{crit}}(z_\ell) \delta_c(c_v)}{d \ln M_\ell} \simeq -0.13 \frac{d \ln \delta_c}{d \ln c_v}.$$

Here ρ_{crit} is the critical density of universe, $\delta_c \equiv \frac{\rho_s}{\rho_{\text{crit}}}$ [34], and $\frac{d \ln \delta_c}{d \ln c_v} \sim 2.67$ for an intermediate lens mass $M_\ell = 10^{4.5} M_\odot$ and $z_\ell = 2$, and it is gradually changing from 2.62 to 2.71 for $c_v \in [30, 75]$ (or alternatively $M_\ell \in [10^3, 10^6] M_\odot$). Therefore, the power-law slope for the dependence of κ_s on M_ℓ is roughly in the range of 0.111–0.123.

C. Lens density profile and the WDM model

WDM halos may have a substantial core in the cases of small particle mass (e.g., $m_p \lesssim 0.5$ keV) [35]; however, many investigations have put constraints on m_p to be larger than a few keV [36]. Here we only consider WDM models with $m_p \gtrsim 3$ keV. In these cases, the core size may be small; thus, we assume that WDM halos follow the NFW profile as CDM halos do.

D. Lens density profile and the SIDM model

SIDM halos may have an isothermal core and follow a piecewise density profile (IC-NFW) as [37]

$$\rho_{\text{SIDM}}(x) = \begin{cases} \rho_{\text{iso}}(x), & \text{for } 0 < x < s, \\ \rho_{\text{NFW}}(x), & \text{for } x \geq s. \end{cases} \quad (14)$$

This profile can be obtained for low-mass halos by solving the Poisson equation (Eq. (2) in Kaplinghat *et al.* [37]), assuming the spherical symmetry and neglecting baryonic effects. We find that $s \sim 0.1$ – 2 by assuming self-interaction cross section $\langle \sigma v \rangle / m_p \sim 1$ – 10^2 cm² km s^{−1} g^{−1} (see Kaplinghat *et al.* [37]). We consider two cases: $s = 0.1$ and $s = 1$.

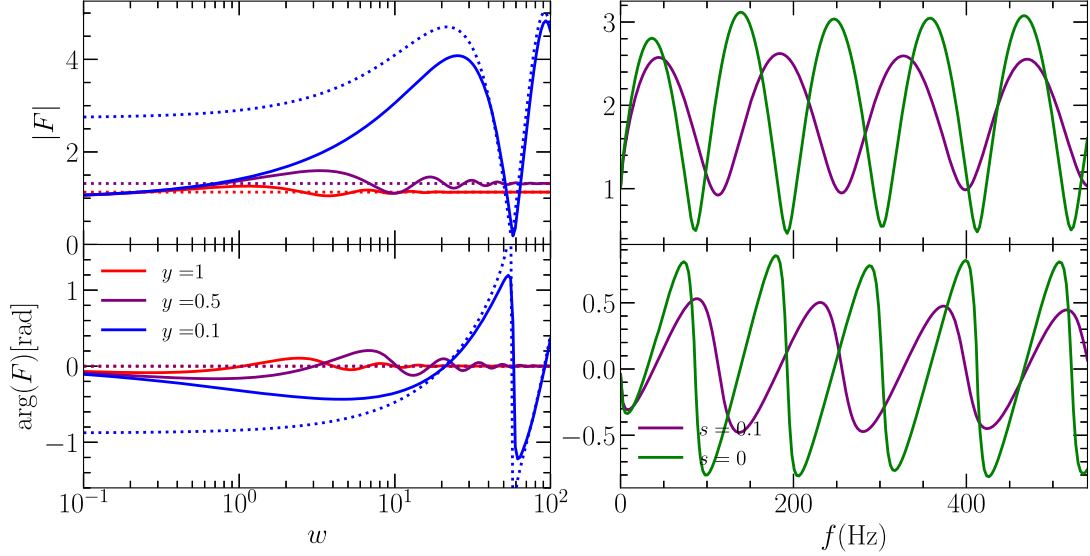


FIG. 1. Magnitude (top panels) and phase (bottom panels) of the amplification factor obtained for pseudo-Jaffe lenses at $z_\ell = 1$. Left panels: $(s, a) = (0.1, 2)$, for which $y_{\text{cr,g}} \approx 0.168$. Right panels: $(s, a) = (0.1, 2)$ or $(0.2, 2)$, $y = 0.2$, $M_\ell = 10^3 M_\odot$, and $\xi_0 = 0.351$ pc (for $s = 0$, $y_{\text{cr,g}} \approx 0.637$). Solid and dotted lines represent the results obtained from wave optics and geometrical optics approximation, respectively.

E. Lensing effects

The differences in density profiles of lenses resulting from different DM models lead to different lensed signals for the same originally unlensed ones. Figures 1 and 2 show the amplification factor for some example lenses with the pseudo-Jaffe, NFW, and IC-NFW profiles. As seen from

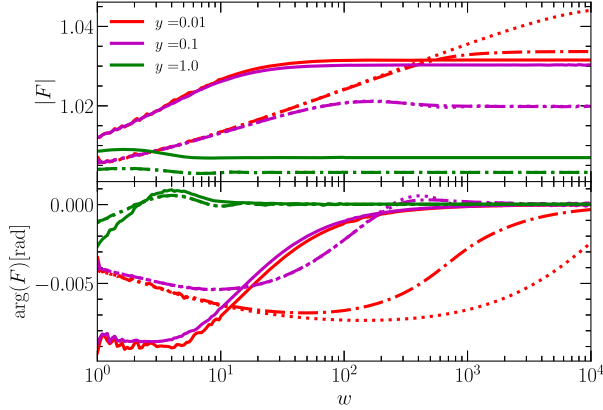


FIG. 2. Magnitude (top panel) and phase (bottom panel) of the amplification factor for the Navarro-Frenk-White (NFW) lens (dotted lines) and the IC-NFW lens with $s = 0.1$ (dotted-dashed line) and $s = 1$ (solid line) at $z_\ell = 1$ with different y values. The masses of all lenses are set as $M_\ell = 10^3 M_\odot$, for which $y = 1/2$ corresponds to 1.27 pc (r_s). The lensed waveforms by the IC-NFW lens, especially at low frequency ($w < 300$), are similar to that by the NFW lens with the same mass when the size of core s is small (e.g., $s = 0.1$); however, it can be significantly different from that by the NFW lens when s is large (e.g., $s = 1$). This suggests that these two different density profiles may be distinguishable from each other by the difference in the lensed GW signals.

these figures, for the pseudo-Jaffe profile, not only can the lensed signals be significantly different from the original one in both amplitude and phase, but also the signals resulting from lenses with or without core are different from each other. The lensed effects obtained for the pseudo-Jaffe profile also have significant differences compared with those obtained for the NFW or NFW-like profile. These suggest that the lensed GW signals can be used to reconstruct/constrain the lens density profile and thus reveal the DM properties. Since the difference between the IC-NFW profile and the NFW profile is only at the region within the core size s , their amplification factors can be significantly different from each other only when $y \lesssim s$.

Here we adopt the methods listed in [27] to numerically integrate Eq. (2) and obtain the diffractive lensing effects of GW signals lensed by minihalos with the NFW/IC-NFW or other profile. We note that Oguri and Takahashi [13] and Choi *et al.* [16] have considered the diffractive lensing effects by NFW halos under the weak lensing approximation, different from our method. The adoption of the weak lensing approximation may lead to some errors in the lensing effect estimates. Dai *et al.* [12] and Gao *et al.* [15] calculated the diffractive lensing effects for lenses with the pseudo-Jaffe or SIS profile, which may not represent the real density profile of DM halos.

III. SNR ANALYSIS OF LENSED/UNLENSED GW SIGNALS

We define an inner product as

$$\langle g|h \rangle \equiv 4\Re \left(\int_0^\infty \frac{\tilde{g}^*(f)\tilde{h}(f)}{S_n(f)} df \right), \quad (15)$$

where \Re represents the real part and S_n the noise power spectral density [12]. Without considering the lensing effect, the SNR of detected signal s_{gw} is

$$\varrho = |\langle h | s_{\text{gw}} \rangle| / \sqrt{\langle s_{\text{gw}} | s_{\text{gw}} \rangle}, \quad (16)$$

where h is the best-matched unlensed template. Considering the lensing effect, the difference between lensed and (original) unlensed signals can be described by

$$\delta\varrho \equiv \sqrt{\langle s_{\text{gw}} - h | s_{\text{gw}} - h \rangle} \quad (17)$$

[23,38], i.e., the “SNR” of difference between two waveforms. The waveforms s_{gw} and h are distinguishable when $\delta\varrho > \delta\varrho_{\text{th}} = 1$ [39]. Sometimes we adopt $\delta\varrho_{\text{th}} = 3$ for higher confidence.

A normalized SNR difference can also be defined as $\delta\hat{\varrho} \equiv \sqrt{\langle s_{\text{gw}} - h | s_{\text{gw}} - h \rangle} / \sqrt{\langle s_{\text{gw}} | s_{\text{gw}} \rangle}$ [12]. If the unlensed waveform is $\tilde{h}(f)$, we assume that the best-fit waveform is $A_{\text{BF}}\tilde{h}(f)$,

$$\delta\hat{\varrho} = \frac{\int_{f_{\min}}^{f_{\max}} \frac{|F(f) - A_{\text{BF}}|^2 |\tilde{h}(f)|^2}{S_n(f)} df}{\int_{f_{\min}}^{f_{\max}} \frac{|\tilde{h}(f)|^2}{S_n(f)} df}, \quad (18)$$

where A_{BF} is a complex constant that we find the best-fit value to make $\delta\varrho$ or $\delta\hat{\varrho}$ smallest. Although phase effect also contributes to $\delta\hat{\varrho}$, we ignore the phase effect in practical calculation and only consider amplitude modulation for convenience. For a lens with the NFW-like profile, the phase of the amplification factor is small ($\lesssim 0.01$ rad); thus, the phase effect can be safely ignored. For a lens with the pseudo-Jaffe profile, the phase of the amplification factor may be significant; ignoring the phase effect may lead to a slight underestimate of the lensing effect and thus the normalized SNR difference $\delta\hat{\varrho}$.

To detect the lensed signal, the lensing effect must be significant enough to satisfy $\delta\hat{\varrho} \geq \delta\varrho_{\text{th}}/\varrho_{\text{unl}}$, where ϱ_{unl} is the SNR of the original unlensed waveform.

For convenience, we use a weight function $W(f) = \frac{|\tilde{h}(f)|^2}{S_n(f)}$ to represent the weight of average; thus, Eq. (18) becomes

$$\delta\hat{\varrho} = \frac{\int_{f_{\min}}^{f_{\max}} |F(f) - A_{\text{BF}}|^2 W(f) df}{\int_{f_{\min}}^{f_{\max}} W(f) df}.$$

Generally, $W(f)$ depends on the redshifted chirp mass $\mathcal{M}_z = \mathcal{M}_0(1 + z_s)$ (\mathcal{M}_0 is the intrinsic chirp mass) and the sensitivity curve of the GW detector.

The redshifted chirp mass \mathcal{M}_z distribution can be obtained by convolving the GW source redshift distribution ($\propto R_{\text{mrg}}(z) \frac{dV}{dz}$) and chirp mass \mathcal{M}_0 distribution. The resulting \mathcal{M}_z distribution has a peak at $\approx 22.2 M_\odot$; therefore, we

adopt the redshifted chirp mass $22.2 M_\odot$ to calculate the weight function $W(f)$ for the ground-based GW detectors for simplicity. If adopting a somewhat different redshifted chirp mass, the weight function should have a different shape, but we have checked it would not lead to a significant changes on the magnitude of $\delta\hat{\varrho}$ (the relative difference $< 20\%$ from $10 M_\odot$ to $100 M_\odot$). For the middle frequency band, we have $|\tilde{h}(f)| \propto f^{-7/6}$ in the inspiral stage of a sBBH merger, which is independent of the chirp mass. Different sources with different chirp masses have the same weight function $W(f)$ for the same GW detectors.

In this paper, we consider a number of current and future ground-based high-frequency GW observatories and middle frequency space GW detectors. These include LIGO, LIGO A+ [40], Einstein Telescope (ET) [41], Cosmic Explorer (CE) [42], Gravitational-wave Lunar Observatory for Cosmology (GLOC) [43], Deci-Hertz Interferometer Gravitational Wave Observatory (DECIGO) [44], and Big Bang Observer (BBO) [45].

Assuming the pseudo-Jaffe profile, $\delta\hat{\varrho}(M_{\ell z}, y)$ can be calculated for any given set of $(M_{\ell z}, y)$. Figures 3 and 4 show $\delta\hat{\varrho}$ as a function of y and $M_{\ell z}$ ($= M_\ell(1 + z_\ell)$), obtained by adopting the GLOC and BBO sensitivity curves, respectively. It is obvious that when y is smaller, $\delta\hat{\varrho}$ is greater. For the same $\delta\hat{\varrho}$, y is usually smaller for more massive minihalos. In the middle-frequency band, y will sharply drop when $M_{\ell z} \simeq 10^3 M_\odot$. If assuming $\delta\varrho(M_{\ell z}, y_{\text{cr}}) = \delta\varrho_{\text{th}}$ as the threshold for detecting the lensing effect, with which the lensing signal is significant enough to be detected if $y \leq y_{\text{cr}}$, while it is not if $y > y_{\text{cr}}$, then we can obtain y_{cr} for any given set of $(\varrho_{\text{unl}}, M_{\ell z})$ by solving the equation $\delta\hat{\varrho}(M_{\ell z}, y_{\text{cr}}) = \frac{\delta\varrho_{\text{th}}}{\varrho_{\text{unl}}}$, which defines the cross section for the diffractive lensing effect to be significant.

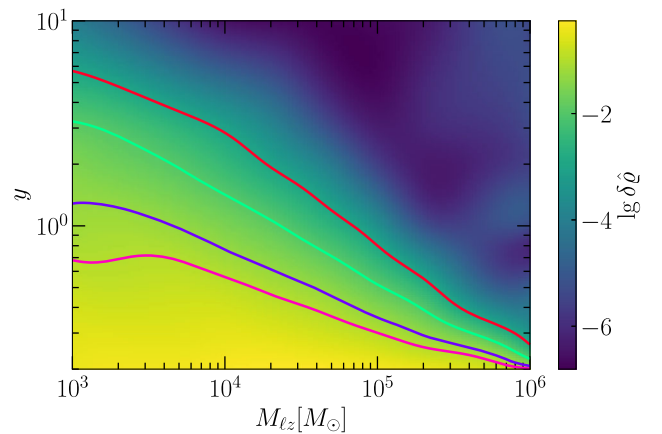


FIG. 3. The distribution of the normalized SNR difference $\delta\hat{\varrho}(M_{\ell z}, y)$ on the $y - M_{\ell z}$ plane obtained by adopting the GLOC sensitivity curve and assuming the pseudo-Jaffe profile for DM halos. The color bar at the right side of the figure indicates the value of $\lg \delta\hat{\varrho}$. The solid color contour lines indicate $\delta\hat{\varrho} = 0.001, 0.01, 0.05$, and 0.1 , respectively (from top to bottom).

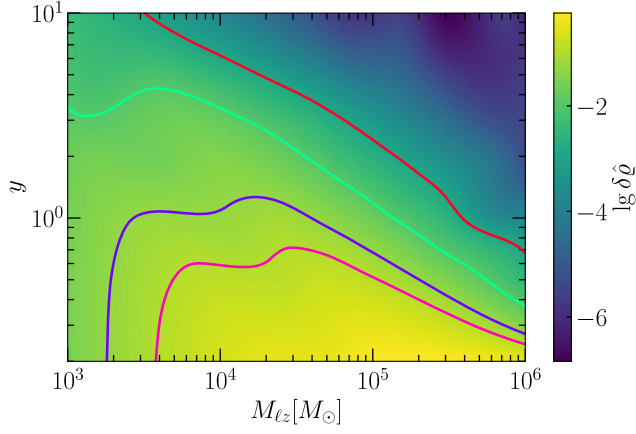


FIG. 4. Legend is similar to that for Fig. 3, but adopting the BBO sensitivity curve.

Assuming the NFW or NFW-like profile, M_{Ez} and κ_s are dependent on $M_\ell \propto M_\ell^{0.926}$ but dependent on z_s and z_ℓ in a complicated way [see Eqs. (12) and (13)]. For simplicity, we check these dependence by generating a large number of lens systems with realistic distributions of M_ℓ , z_ℓ , and z_s . The probability distribution of z_s of sBBH mergers given by the merger rate density distribution $p(z_s) \propto R_{\text{mrg}}(z_s) \frac{dV}{dz_s}$ (see Sec. IV for detailed description). There is no significant difference for the halo mass function (HMF) between $z_\ell = 0$ and 5 (see Fig. 10 below in Sec. IV) and the number density of source peaks at $z_s \sim 2$. Thus we can assume $n_\ell(z_\ell) \sim \text{constant}$, for simplicity. The conditional probability distribution for lens is $p(D_\ell | D_s) dD_\ell \propto n_\ell \pi \theta_E^2 D_\ell^2 dD_\ell$, where $\theta_E^2 \propto \frac{D_{\ell s}}{D_s D_\ell}$; thus, $p(z_\ell | z_s) \propto n_\ell \pi \theta_E^2 D_\ell^2 \frac{dD_\ell}{dz_\ell} = n_\ell \pi D_{\text{eff}}^2 \frac{c}{H(z_\ell)}$. According to $p(z_s)$ and $p(z_\ell | z_s)$, we generate 1000 lens-sources systems with different M_ℓ ($\in [10^3, 10^{12}] M_\odot$), z_s ($\in [0, 8]$) [46] to check the dependence of M_{Ez} and κ_s on M_ℓ , z_ℓ ($\in [0, z_s]$), and z_s . For each set of (z_ℓ, z_s, M_ℓ) , we can calculate the corresponding M_{Ez} and κ_s . For lens halos with the NFW profile and the IC-NFW profile ($s = 0.1$ or $s = 1$), they roughly have the same M_{Ez} and κ_s if (M_ℓ, z_ℓ, z_s) are the same. We find that M_{Ez} and κ_s mainly depend on M_ℓ , and the differences in z_ℓ and z_s of the lens systems introduce some scatters to the main relationship between M_{Ez} (or κ_s) and M_ℓ . We fit the dependence of either M_ℓ or κ_s on M_ℓ as a power law with a scatter reflecting the effects of z_ℓ and z_s , and find $M_{Ez}(M_\ell) \approx 28.2 M_\odot (M_\ell / M_\odot)^{0.928}$ with a scatter of $\sigma_{\lg M_{Ez}/M_\odot} = 0.221$, and $\kappa_s \approx 0.00510 (M_\ell / M_\odot)^{0.121}$ with a scatter of $\sigma_{\lg \kappa_s} = 0.136$. Apparently, the index 0.928 is consistent with the estimate in Eq. (12), and the redshift distributions of z_ℓ and z_s only lead to a small scatter [the factors $g_1(z_\ell, z_s)$ and $g_2(z_\ell, z_s)$ in Eqs. (12) and (13)] to the relationship between M_{Ez} and M_ℓ . For simplicity, we thus ignore the dependence on z_ℓ and z_s for when estimating the cross section for those “detectable” lensed events below.

For minihalo lenses with the NFW (or NFW-like) profiles, $\delta\hat{q}$ can be estimated, as a function of halo mass

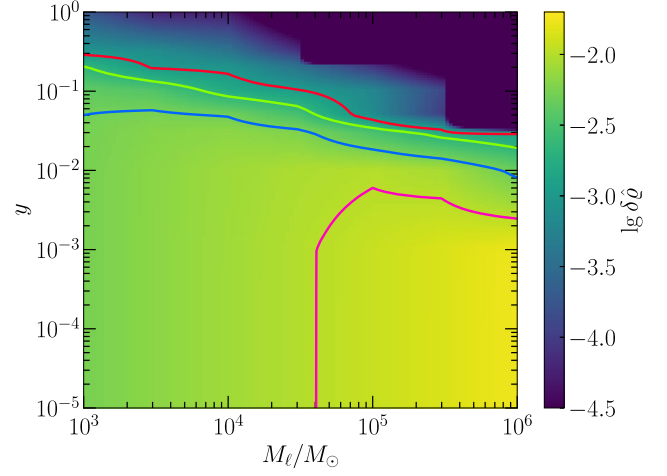


FIG. 5. Legend is similar to that for Fig. 3, but adopting the NFW density profile for minihalos and the GLOC sensitivity curve. The solid color contour lines indicate $\delta\hat{q} = 0.001, 0.002, 0.005$, and 0.01 , respectively (from top to bottom).

M_ℓ ($\in [10^3, 10^6] M_\odot$) and y ($\in [10^{-5}, 1]$). We adopt the above fitting relationships between M_{Ez} (or κ_s) and M_ℓ without considering the scatters due to the distributions of z_ℓ and z_s , for simplicity. If we set the SNR difference $\delta\hat{q}_{\text{th}} = 1$ as the threshold for detectable lensed events, then we can obtain the threshold for y parameter, i.e., y_{cr} , by solving the equation $\delta\hat{q}(y_{\text{cr}}, M_\ell) = \delta\hat{q}_{\text{th}}/q_{\text{unl}}$. Figure 5 shows $\delta\hat{q}$ as a function of y and M_ℓ for the NFW profile by adopting GLOC sensitivity curve as an example. Figures 6 and 7 show the distributions of $y_{\text{cr}}(\delta\hat{q}, M_\ell)$ on the $M_\ell - \delta\hat{q}$ plane for the NFW profile by adopting the GLOC and BBO sensitivity curves, as examples for the high-frequency ground-based GW observatories and the midfrequency-space GW detectors, respectively. In both figures, the

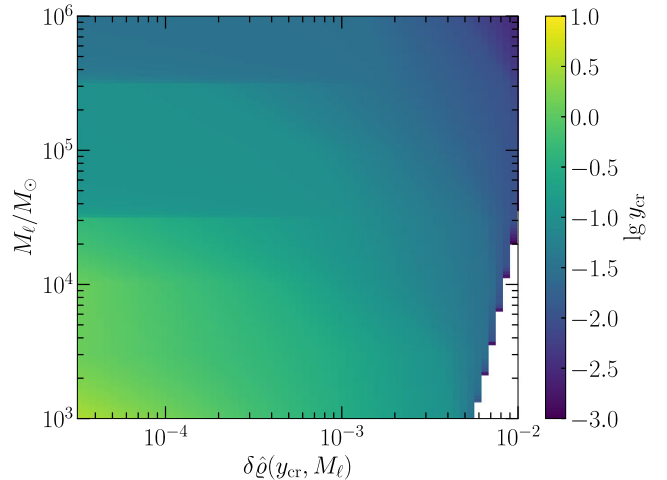


FIG. 6. The “detectable” threshold y_{cr} of the diffractive lensing effect by minihalos with M_ℓ ($\in [10^3, 10^6] M_\odot$) and the SNR difference of $\delta\hat{q}$ obtained by adopting the NFW profile for minihalos and the GLOC sensitivity curve. The blank region represents $y_{\text{cr}} \rightarrow 0$.

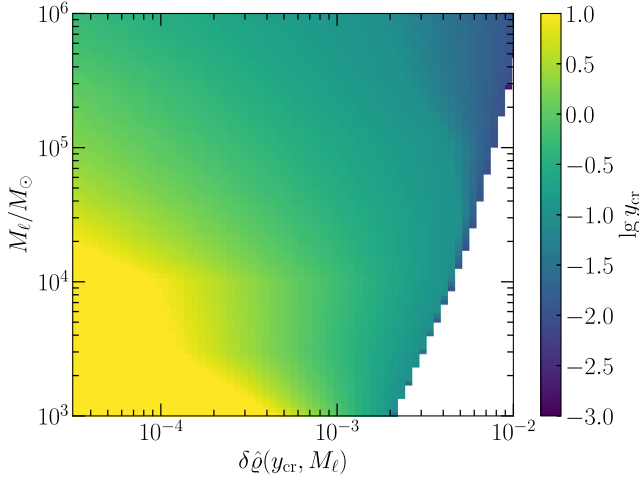


FIG. 7. Legend is similar to that for Fig. 6 except that the BBO sensitivity curve is adopted.

smaller lens mass and the smaller $\delta\hat{Q}(y_{\text{cr}}, M_\ell)$, the relatively larger y_{cr} . By comparison of these two figures, it can be clearly seen that y_{cr} obtained for the BBO sensitivity curve is substantially larger than that for the GLOC sensitivity curve because the diffraction effect is more significant in the middle-frequency band than that in the high-frequency band for those minihalos. Generally, the y_{cr} is greater for smaller $\delta\hat{Q}$.

For the IC-NFW profile with $s = 0.1$ and $s = 1$, we also calculate $\delta\hat{Q}$ for different halo masses M_ℓ ($\in [10^3, 10^6] M_\odot$) and y ($\in [10^{-5}, 1]$). Figures 8 and 9 show the distributions of $y_{\text{cr}}(\delta\hat{Q}, M_\ell)$ for minihalos with the IC-NFW density profile with $s = 0.1$ on the $\delta\hat{Q} - M_\ell$ plane by adopting the GLOC and BBO sensitivity curves, respectively. For the ground-based GW detectors in the high-frequency band, y_{cr} for minihalos with the IC-SIDM profile (Fig. 8) is significantly smaller than that for those with the NFW profile (Fig. 6), especially at large $M_\ell \sim 10^6 M_\odot$. The reason for this is that

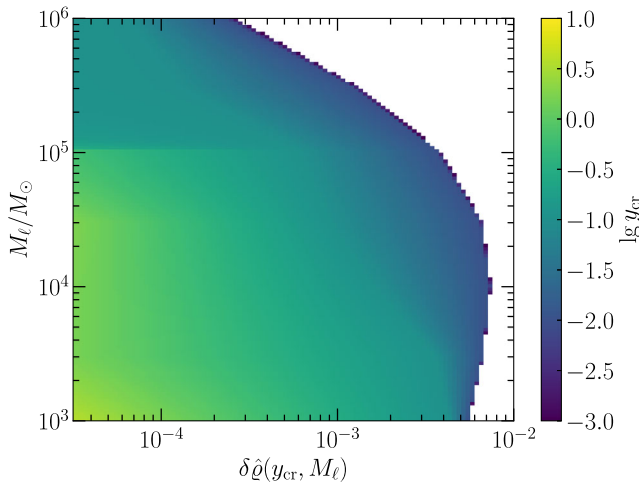


FIG. 8. Legend is similar to that for Fig. 6 except that the SIDM density profile is adopted.

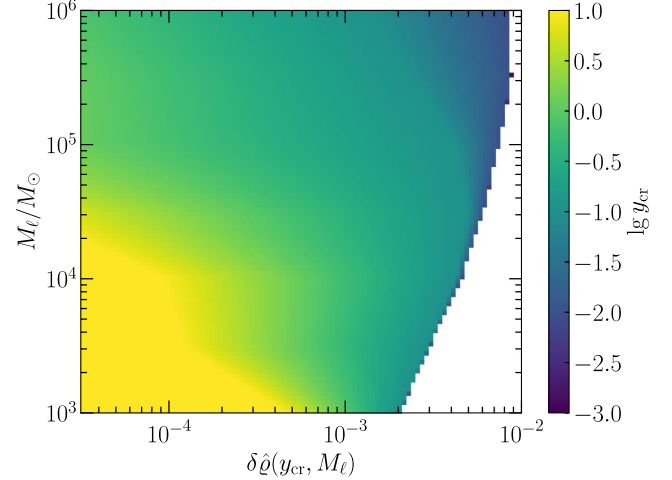


FIG. 9. Legend is similar to that for Fig. 7 except that the SIDM density profile is adopted.

the amplification factors of those minihalo lenses with the IC-NFW profile and the NFW profile have significant difference in the high-frequency band. The former ones become flat when f (or w) is sufficiently large for small $y \lesssim s$ (see Fig. 2), while the latter ones still increase with increasing f (or w). This is also the reason why the lensing rate of SIDM is smaller than CDM with NFW profile for ground-based detectors that will be introduced in later sections. However, for the space GW detectors in the middle-frequency band, y_{cr} for minihalos with the IC-NFW profile (Fig. 9) is similar to that for those with the NFW profile (Fig. 7). The reason is that the amplification factors for minihalos with the NFW profile and those with the IC-NFW profile ($s = 0.1$) are almost the same in the middle-frequency band even when y is small. Therefore, their lensing rates are also similar to each other as shown in Sec. IV. If the IC-NFW profile has a larger core, e.g., $s = 1$, the resulting y_{cr} will be significantly smaller than that from the NFW profile at both high-frequency and middle frequency bands.

The cross section for minihalos in the wave optics regime is substantially larger than that in the geometrical limit (zero or very small depending on the density profile and lens masses; see Ref. [47]); thus, the diffractive lensing rate of GW sources by minihalos is much larger than the corresponding strong lensing rate in the geometrical optics regime. Here we ignore the strong lensing effect as its cross section for minihalos is negligible comparing with that of the diffractive lensing effect. We adopt the critical value y_{cr} to infer the cross section $\sigma = \pi(\xi_0(M_\ell)/D_\ell)^2 y_{\text{cr}}^2$ and calculate the diffractive lensing event rate.

Given the lensing cross sections, the optical depth for a GW source at z_s lensed by halos is

$$\tau(Q, z_s) = \frac{1}{4\pi} \int_0^{z_s} dz_\ell \int dM_\ell \pi(\xi_0(M_\ell)/D_\ell)^2 y_{\text{cr}}^2 \frac{dn}{dM_\ell} \frac{dV^c}{dz_\ell}, \quad (19)$$

where dn/dM_ℓ is the HMF and can be calculated using the PYTHON program `hmf` [48], V^c is the cosmic comoving volume, the integration ranges for z_ℓ and M_ℓ are $(0, z_s)$ and $(10^3, 10^6) M_\odot$, respectively. For lower-mass halos, the lensing effect is substantially weaker, while for higher-mass halos, they may not act in the diffraction regime and their density profiles may be significantly affected by baryonic processes.

IV. EXPECTED LENSING RATE

After defining the threshold of cross section y_{cr} from SNR analysis, we can calculate the expected lensing rate for current and future GW detectors at the high-frequency band (Sec. IV A) and the middle-frequency band (Sec. IV B), respectively. Finally, our results are presented in Sec. IV C.

A. High-frequency band

The differential event rate of GW sources (e.g., sBBH mergers) is given by

$$\frac{d^3 \dot{N}}{dz d\mathcal{M} dq} = P_\ell(q|z, \mathcal{M}_0) \frac{R_{\text{mrg}}(\mathcal{M}_0; z) dV^c}{(1+z)} \frac{dV^c}{dz}, \quad (20)$$

where $R_{\text{mrg}}(\mathcal{M}_0; z) = p(\mathcal{M}_0|z) R_{\text{mrg}}(z)$ is the merger rate density (MRD) for events with chirp mass \mathcal{M}_0 at z [20], and $P_\ell(q|z, \mathcal{M}_0)$ is the conditional probability distribution of SNR at z and \mathcal{M}_0 [20,49]. We estimate the sBBH MRD by using the “R3:1” model in [50], with which 75% sBBHs are formed from evolution of field binary stars and the rest originated from dynamical interactions, but rescale it to the latest constraint on the local MRD [51]. This model is adopted as its resulting MRD evolution and chirp mass distribution are more or less consistent with current LIGO/Virgo observations. There are still some uncertainties in the constraints on the MRD and its evolution [51], which directly introduce errors into the lensing rate estimates, but by a factor < 2 .

The detection rate of lensed GW events is

$$\dot{N}_\ell(> q_{\text{th}}) \simeq \int_{q_{\text{th}}}^\infty dq \iint dz_s d\mathcal{M}_0 p_\ell(q, z_s) \frac{d^3 \dot{N}}{dz_s d\mathcal{M}_0 dq}, \quad (21)$$

where the lensing probability $p_\ell(q, z_s) = 1 - e^{-\tau(q, z_s)}$. The total detection rate of GW events is

$$\dot{N}_s(> q_{\text{th}}) \simeq \int_{q_{\text{th}}}^\infty dq \iint dz_s d\mathcal{M}_0 \frac{d^3 \dot{N}}{dz_s d\mathcal{M}_0 dq}. \quad (22)$$

Here we ignore the magnification bias as the amplification amplitude is close to 1 for most lensed events in the wave optics regime.

B. Middle-frequency band

For the middle-frequency band GW detectors, the target GW sources are no longer the sBBH mergers, but the inspiraling sBBHs. They are continuous GW sources and will last for a long time. The differential event number is [50,52]

$$\frac{d^3 N}{dz d\mathcal{M}_0 dq} = P_\ell(q|z, \mathcal{M}_0) \frac{R_{\text{mrg}}(\mathcal{M}_0, z) dV^c}{(1+z)} \frac{dV^c}{dz} \cdot \int_{\log_{10} f_{\text{min}}}^{\log_{10} f_{\text{max}}} \frac{dt}{d \log_{10} f} d \log_{10} f, \quad (23)$$

where

$$\frac{dt}{d \log_{10} f} = \frac{5 \ln 10}{96} \pi^{-8/3} \left[\frac{G \mathcal{M}_0 (1+z)}{c^3} \right]^{-5/3} f^{-8/3}.$$

For the middle-frequency GW detectors, the targeted frequency range is normally from 0.1 to 10 Hz. In Eq. (23), we simply set $f_{\text{max}} = 10$ Hz, and the slightly different value for f_{max} does not affect the integral value much as the residence timescale for sBBHs $\propto f^{-8/3}$. For a given observation period Δt , those events that can sweep over the targeted frequency range of the middle-frequency GW detectors can have the frequency at the start time of the observation as

$$f_{\text{min}}^{-8/3} - f_{\text{max}}^{-8/3} = 8 \cdot \frac{32}{5} \pi^{8/3} \left(\frac{G \mathcal{M}_z}{c^3} \right)^{5/3} \Delta t,$$

and thus

$$f_{\text{min}} \approx 0.0335 \text{ Hz} \left(\frac{\mathcal{M}_z}{22.2 M_\odot} \right)^{5/8} \left(\frac{\Delta t}{1 \text{ yr}} \right)^{-3/8}.$$

If $\Delta t > 1$ yr, we have $f_{\text{min}} < 0.1$ Hz, which means that we can also roughly define the detection rate as $\frac{1}{\Delta t} d^3 N / dz d\mathcal{M}_0 dq$, and the SNR can be estimated as

$$\rho = 8\Theta \frac{r_{\text{det}}}{d_L} \left(\frac{\mathcal{M}_z}{1.2 M_\odot} \right)^{5/6}.$$

Here d_L is the luminosity distance, Θ is the orientation function [49], and we denote

$$r_{\text{det}}^2 \equiv \frac{5}{192\pi} \left(\frac{3G}{20} \right)^{5/3} \frac{M_\odot^2}{c^3} \int_{f_{\text{min,det}}}^{f_{\text{max,det}}} \frac{(\pi M_\odot)^2}{(\pi f M_\odot)^{7/3} S_n(f)} df,$$

with $f_{\text{max,det}} = 10$ Hz and $f_{\text{min,det}} = 0.01$ Hz. We adopt the sensitivity curves $S_n(f)$ for DECIGO and BBO as those given in [53].

TABLE I. Expected diffraction lensing rate \dot{N}_ℓ (yr^{-1}) of stellar sBBH mergers/inspiral for LIGO, LIGO A+, ET, CE, GLOC, DECIGO, and BBO, estimated by assuming different DM models (CDM; WDM with particle mass of 30, 10, and 3 keV, respectively; and SIDM), and different density profiles (pseudo-Jaffe, NFW, and IC-NFW) for halos. The second column indicates the expected total sBBH detection rates by different GW detectors with a SNR threshold of $q_{\text{th}} = 8$. The last row (for BBO) and the last third row (for DECIGO) show the results obtained by assuming a conservative SNR difference threshold of $\delta q_{\text{th}} = 3$, while other rows show the results obtained by assuming $\delta q_{\text{th}} = 1$.

Detector	\dot{N}_s (yr^{-1})	\dot{N}_ℓ (yr^{-1})									
		pseudo-Jaffe					NFW				
		WDM					WDM				
		CDM	30 keV	10 keV	3 keV	CDM	30 keV	10 keV	3 keV	s = 0.1	s = 1
LIGO	971	0.344	0.0688	0.0133	0.00143	1.85×10^{-7}	5.09×10^{-8}	9.53×10^{-9}	1.01×10^{-9}	8.52×10^{-8}	6.18×10^{-10}
LIGO A+	2502	1.41	0.303	0.0599	0.00640	6.44×10^{-7}	1.80×10^{-7}	3.38×10^{-8}	3.58×10^{-9}	2.88×10^{-7}	2.45×10^{-9}
ET	3.26×10^4	207	31.7	5.49	0.563	0.00421	0.00138	2.64×10^{-4}	2.78×10^{-5}	0.00125	8.93×10^{-6}
CE	3.82×10^4	274	37.8	6.47	0.661	0.288	0.0899	0.0169	0.00172	0.0980	4.69×10^{-4}
GLOC	3.90×10^4	893	115	18.2	1.84	1.02	0.243	0.0437	0.00436	0.585	0.00223
DECIGO	3.92×10^4	3640	516	77.6	7.76	9.67	3.25	0.601	0.0604	9.61	2.37
BBO	3.97×10^4	1112	193	30.7	3.09	0.0778	0.0306	0.00634	6.15×10^{-4}	0.0745	0.0132
		8022	996	146	14.5	189	44.1	7.81	0.803	192	88.2
		3281	448	66.9	6.68	5.66	1.96	0.367	0.0376	5.48	0.906

C. Results

We estimate the number of detectable lensed GW events for different GW detectors including the ground-based GW observatories (LIGO, LIGO A+, ET, CE, and GLOC) and the middle-frequency GW detectors (DECIGO and BBO), by assuming different DM models and halo density profiles. Our results are listed in Table I and shown in Fig. 10. Apparently, the predicted detectable lensing event rates for a given GW detector can differ by orders of magnitude if assuming different DM models, because of the differences in both the resulting halo abundance and density profiles. As seen from the top left panel of Fig. 10, the HMF at the low-mass end ($\sim 10^3$ – $10^6 M_\odot$) resulting from the WDM model (with $m_p \lesssim 30$ keV) is more than one to two orders of magnitude smaller than that from the CDM model. Other panels of Fig. 10 show the differential detectable lensing rates by different GW detectors. For the third-generation GW detectors ET, CE, and GLOC, and the middle-frequency GW detectors DECIGO and BBO, it seems that the expected rate of all the detectable GW events does not increase significantly with increasing sensitivity, mainly caused by the fact that most GW events at redshift $z \lesssim 5$ will be “detected” by these GW detectors as they are all sufficiently sensitive. Nevertheless, the SNRs of all those detectable GW events will be significantly enhanced with increasing GW detection sensitivity. Therefore, those GW detectors with high sensitivity can detect more lensed GW events because the lensed signal can be easier identified via the SNR difference threshold.

If DM is cold, the detection rate of GW events lensed by CDM minihalos with NFW profiles is estimated to be $\sim 1.85 \times 10^{-7}$, 6.44×10^{-7} , 0.00421, 0.288, 1.02, 9.67, and 189 yr^{-1} for LIGO, LIGO A+, ET, CE, GLOC, DECIGO, and BBO, respectively, while it is ~ 0.344 , 1.41, 207, 274, 893, 3640, and 8022 yr^{-1} , respectively, if assuming the pseudo-Jaffe profile. The reason is that the pseudo-Jaffe halos are more concentrated than those NFW ones, and thus have relatively larger cross sections for diffractive lensing. According to these estimates, it is expected that tens to hundreds of such lensed events may be detected in the era of ET/CE/GLOC, and even more than thousands of lensed events can be detected for DECIGO and BBO.

If DM is warm with $m_p = 30$ keV, then this detection rate is $\sim 5.09 \times 10^{-8}$, 1.80×10^{-7} , 0.00138, 0.0899, 0.243, 3.25, and 44.1 yr^{-1} (or 0.0688, 0.303, 31.7, 37.8, 115, 516, and 996 yr^{-1}) for LIGO, LIGO A+, ET, CE, GLOC, DECIGO, and BBO, respectively, by adopting the NFW (or pseudo-Jaffe) profile. These expected rates are substantially smaller than those from the CDM model mainly because the abundance of minihalos resulting from the WDM model is substantially smaller than that from the CDM model. Assuming the WDM model with $m_p \gtrsim 10$ keV, DECIGO (BBO) is expected to detect about more than

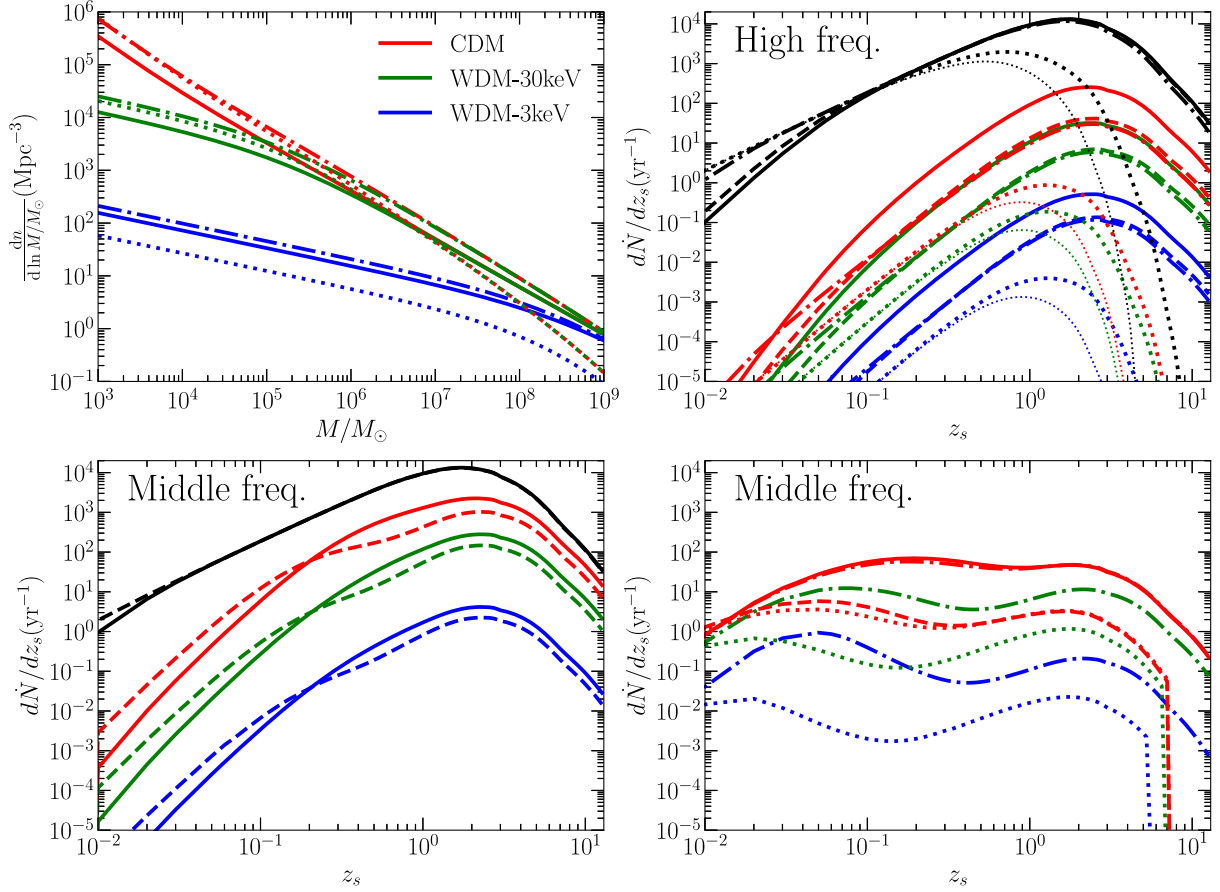


FIG. 10. The halo mass function (top left panel) and the differential diffractive lensing rates of sBBH mergers (other panels) estimated for different DM models. Red, green, and blue lines represent those obtained from the models assuming CDM, WDM with mass of 30 keV (WDM-30 keV), and 3 keV (WDM-3 keV), respectively. Top left panel: the solid, dotted-dashed, and dotted lines show the halo mass functions at $z = 0, 5$, and 10 , respectively. Top right panel: the black lines show the total GW event rates; the thin dotted, thick dotted, thick dashed, thick dotted-dashed, and thick solid lines represent those obtained by using the LIGO, LIGO A+, ET, CE, and GLOC sensitivity curves, respectively. The red, green, and blue lines represent the differential lensing rates obtained from the CDM, WDM-30 keV, and WDM-3 keV models, respectively. For illustration, the pseudo-Jaffe profile is adopted for all DM halos [with $(s, a) = (0.1, 2)$] for the results showing in this panel. Bottom left panel: the black lines shows the total GW event rate in the middle-frequency band; the solid and dashed lines represent the differential lensing rates obtained by using the BBO and DECIGO sensitivity curves, respectively, and the DM halos are also assumed here to follow the pseudo-Jaffe profile. Bottom right panel: the red, green, and blue lines represent the estimated differential lensing rates for the CDM/SIDM, WDM-30 keV, and WDM-3 keV model, respectively, where the red dotted-dashed line and the red dotted line represent the results for the CDM model, and the red solid line and the red dashed line represent the results for the SIDM model. The solid line and the dotted-dashed line represent the rates obtained by using the BBO sensitivity curve; the dashed line and the dotted line both represent those obtained by using the DECIGO sensitivity curve. For this panel, the DM halos are assumed to follow the NFW profile in the CDM and WDM models, but an IC-NFW profile with $s = 0.1$ [see Eq. (14)] in the SIDM model.

one (several) lensed GW events per year. However, one would not expect to detect any diffractively lensed GW event by GLOC and DECIGO within a reasonable observation period, if m_p is much smaller ($\ll 10$ keV).

As for the SIDM model, the expected lensing rate could be different for different core size s . If the core size $s = 0.1$, the expected lensing rate detected by DECIGO/BBO is similar to that expected from the CDM model because the lensing effects of the IC-NFW halos are almost the same as that of NFW lens. But, if we have detected a lensed event with $y \lesssim 0.1$, it is still possible to distinguish different lens

profiles by the lensed waveform. For the SIDM model, if the lenses follow the IC-NFW profile with large s , e.g., $s = 1$, the lensing rate could be significantly less than that of the NFW lens or the IC-NFW lens with $s = 0.1$. The significant difference between the lensed GW waveforms by the IC-NFW halos and that of the NFW halos can also be used to distinguish the SIDM model with $s = 1$ from the CDM model (Fig. 2).

Note that we set the threshold for the lensed GW signatures to be identifiable as $\delta\varphi \geq \delta\varphi_{\text{th}} = 1$ above. However, one may also set a more conservative threshold,

for which the estimate lensing rates should decrease substantially and the confidence for the defined detectable event would be much higher. In Table I, the last third and the last rows list the estimates of the corresponding lensing rates for DECIGO and BBO by adopting a conservative threshold of $\delta q_{\text{th}} = 3$. Apparently, under this more stringent threshold the estimated lensed GW event detection rates decrease by a factor of several to a hundred compared with those under the threshold of $\delta q_{\text{th}} = 1$. However, it is still promising for BBO to detect some lensed systems and thus possible to distinguish different DM models.

Note here the estimation for the expected lensing rate is also affected by other factors, such as the uncertainty in the sBBH merger rate, the choice of the threshold for determining the diffraction cross section, etc. For example, if there are many more sBBH mergers at high redshift than that predicted by the simple model adopted in this paper, the lensing rate can be higher than those listed in Table I. The phase effect is ignored for identifying the lensing events via δq in this paper. For a given diffractive lensing system, we expect to obtain a larger δq by considering both the amplitude and phase effects and thus may result in a larger detection rate of the lensing events than those obtained in the present paper. Furthermore, we estimate the lensing probability and lensing rate for main halos but do not consider subhalos. Low-mass subhaloes may also contribute to the lensing rate in this mass range, 10^3 – $10^6 M_\odot$. In addition, the multiple deflections from weak lensing of all kinds of celestial objects may also contribute unknown noise to signal detection, which needs to be considered in future studies.

V. SUMMARY

We have systematically investigated the lensed GW signal by minihalos (10^3 – $10^6 M_\odot$) in the wave optics regime. We estimate the detection rate of such lensing events by current and future GW detectors assuming different DM models, and we find that the detection rate significantly depends on the DM nature. The reasons for this dependence are the different abundances and the different density profiles of small DM halos resulting from different DM models.

We find that the current and future ground-based GW observatories, such as LIGO, LIGO A+, and ET, are almost unlikely to detect minihalos (with the NFW profile) via the gravitational lensing of GW within a limited observational period (e.g., less than 10 yr). CE and GLOC may detect several to tens of GW events diffractively lensed by CDM

minihalos (with the NFW profile) over an observation period of 10 yr or more. If the minihalo density profiles have a much steeper (inner) slope than the NFW-like profile, such as the pseudo-Jaffe profile, ET, CE, and GLOC are expected to detect a significant number of minihalos via the diffractive lensing of GWs. With the detection of these lens events, one may be able to distinguish different kinds of DM halo density profiles using the lensed GW signals.

Assuming that the minihalos resulting from the CDM model follow the NFW density profile, it is expected that the DECIGO/BBO may detect several/hundreds of GW events per year, which are diffractively lensed by minihalos. Even GLOC can also detect one event per year. For the WDM model (> 10 keV) with the same profiles, it is still expected that the DECIGO/BBO may detect about one/several events per year. As for the SIDM model, the expected lensing rates depend on the choice of the core size for those halos (describing the IC-NFW profile). If the core size is small (e.g., $s = 0.1$), the expected lensing rates are similar to those from the CDM model (halos with the NFW profile), especially in the middle-frequency band. If the core size is large (e.g., $s = 1$), the expected lensing rates are smaller than those from the CDM model (halos with the NFW profile). However, it is still promising to detect several (tens of) events by the middle-frequency detectors like DECIGO (BBO) if the core size of the SIDM halos is not too large ($s \leq 1$). These estimates on the detection rates of diffractively lensed GW events by minihalos suggest that the DM nature, either cold, warm, or self-interacting, may be significantly constrained via the detection of the diffractively lensed GW events by future GW detectors. In the meantime, the density profiles of minihalos as lenses may also be revealed via the lensed GW signals, which would provide further information on the DM nature.

ACKNOWLEDGMENTS

We thank the anonymous referee for helpful comments and suggestions. We also thank Shun-Sheng Li, Liang Dai, and Shude Mao for stimulating discussions. This work is partly supported by the National Key Program for Science and Technology Research and Development (Grant No. 2020YFC2201400), the National Natural Science Foundation of China (Grants No. 11690024, No. 11873056, and No. 11991052), and the Strategic Priority Program of the Chinese Academy of Sciences (Grant No. XDB 23040100).

- [1] S. Tulin and H.-B. Yu, *Phys. Rep.* **730**, 1 (2018).
- [2] J. Liu, X. Chen, and X. Ji, *Nat. Phys.* **13**, 212 (2017).
- [3] J. Bahcall, T. Piran, and S. Weinberg, *Dark Matter in the Universe*, 2nd ed. (World Scientific, Singapore, 2004).
- [4] D. N. Spergel and P. J. Steinhardt, *Phys. Rev. Lett.* **84**, 3760 (2000).
- [5] P. Bode, J. P. Ostriker, and N. Turok, *Astrophys. J.* **556**, 93 (2001).
- [6] L. Hui, J. P. Ostriker, S. Tremaine, and E. Witten, *Phys. Rev. D* **95**, 043541 (2017).
- [7] O. Newton, M. Leo, M. Cautun, A. Jenkins, C. S. Frenk, M. R. Lovell, J. C. Helly, and A. J. Benson, *arXiv:2011.08865*; R. Kennedy, C. Frenk, S. Cole, and A. Benson, *Mon. Not. R. Astron. Soc.* **442**, 2487 (2014).
- [8] J. F. Navarro, V. R. Eke, and C. S. Frenk, *Mon. Not. R. Astron. Soc.* **283**, L72 (1996).
- [9] A. Benítez-Llambay, C. S. Frenk, A. D. Ludlow, and J. F. Navarro, *Mon. Not. R. Astron. Soc.* **488**, 2387 (2019).
- [10] S. Shen, P. Madau, C. Conroy, F. Governato, and L. Mayer, *Astrophys. J.* **792**, 99 (2014); T. Sawala, C. S. Frenk, A. Fattahi, J. F. Navarro, T. Theuns, R. G. Bower, R. A. Crain, M. Furlong, A. Jenkins, M. Schaller, and J. Schaye, *Mon. Not. R. Astron. Soc.* **456**, 85 (2016).
- [11] A. Ulmer and J. Goodman, *Astrophys. J.* **442**, 67 (1995).
- [12] L. Dai, S.-S. Li, B. Zackay, S. Mao, and Y. Lu, *Phys. Rev. D* **98**, 104029 (2018).
- [13] M. Oguri and R. Takahashi, *Astrophys. J.* **901**, 58 (2020).
- [14] M. Oguri and R. Takahashi, *arXiv:2204.00814*.
- [15] Z. Gao, X. Chen, Y.-M. Hu, J.-D. Zhang, and S.-J. Huang, *Mon. Not. R. Astron. Soc.* **512**, 1 (2022).
- [16] H. G. Choi, C. Park, and S. Jung, *Phys. Rev. D* **104**, 063001 (2021).
- [17] J. Urrutia and V. Vaskonen, *Mon. Not. R. Astron. Soc.* **509**, 1358 (2022).
- [18] S. Cao, J. Qi, M. Biesiada, T. Liu, J. Li, and Z.-H. Zhu, *Mon. Not. R. Astron. Soc.* **502**, L16 (2021).
- [19] S. Cao, J. Qi, Z. Cao, M. Biesiada, W. Cheng, and Z.-H. Zhu, *Astron. Astrophys.* **659**, L5 (2022).
- [20] S.-S. Li, S. Mao, Y. Zhao, and Y. Lu, *Mon. Not. R. Astron. Soc.* **476**, 2220 (2018).
- [21] M. Biesiada, X. Ding, A. Piórkowska, and Z.-H. Zhu, *J. Cosmol. Astropart. Phys.* **10** (2014) 080.
- [22] C. R. Keeton, *arXiv:astro-ph/0102341*.
- [23] S. Jung and C. S. Shin, *Phys. Rev. Lett.* **122**, 041103 (2019).
- [24] L. Dai and T. Venumadhav, *arXiv:1702.04724*.
- [25] S. Hou, X.-L. Fan, K. Liao, and Z.-H. Zhu, *Phys. Rev. D* **101**, 064011 (2020).
- [26] J. M. Diego, *Phys. Rev. D* **101**, 123512 (2020).
- [27] X. Guo and Y. Lu, *Phys. Rev. D* **102**, 124076 (2020).
- [28] T. T. Nakamura and S. Deguchi, *Prog. Theor. Phys. Suppl.* **133**, 137 (1999).
- [29] W. Jaffe, *Mon. Not. R. Astron. Soc.* **202**, 995 (1983).
- [30] J. F. Navarro, C. S. Frenk, and S. D. M. White, *Astrophys. J.* **462**, 563 (1996).
- [31] M. Oguri, A. Taruya, and Y. Suto, *Astrophys. J.* **559**, 572 (2001).
- [32] J. Wang, S. Bose, C. S. Frenk, L. Gao, A. Jenkins, V. Springel, and S. D. M. White, *Nature (London)* **585**, 39 (2020).
- [33] R. Takahashi, *Astron. Astrophys.* **423**, 787 (2004).
- [34] Saas-Fee Advanced Course 33: Gravitational Lensing: Strong, Weak and Micro (Springer Berlin, Heidelberg, 2006).
- [35] M. R. Lovell, C. S. Frenk, V. R. Eke, A. Jenkins, L. Gao, and T. Theuns, *Mon. Not. R. Astron. Soc.* **439**, 300 (2014).
- [36] J.-W. Hsueh, W. Enzi, S. Vegetti, M. Auger, C. D. Fassnacht, G. Despali, L. V. Koopmans, and J. P. McKean, *Mon. Not. R. Astron. Soc.* **492**, 3047 (2020).
- [37] M. Kaplinghat, S. Tulin, and H.-B. Yu, *Phys. Rev. Lett.* **116**, 041302 (2016).
- [38] K. Liao, S. Tian, and X. Ding, *Mon. Not. R. Astron. Soc.* **495**, 2002 (2020).
- [39] L. Lindblom, B. J. Owen, and D. A. Brown, *Phys. Rev. D* **78**, 124020 (2008).
- [40] B. P. Abbott *et al.* (KAGRA, LIGO Scientific, and Virgo Collaborations), *Living Rev. Relativity* **23**, 3 (2020).
- [41] S. Hild, *Classical Quantum Gravity* **29**, 124006 (2012).
- [42] D. Reitze (LIGO Laboratory: California Institute of Technology, LIGO Laboratory: Massachusetts Institute of Technology, LIGO Hanford Observatory, and LIGO Livingston Observatory), *Bull. Am. Astron. Soc.* **51**, 141 (2019), <https://baas.aas.org/pub/2020n3i141/release/1>.
- [43] K. Jani and A. Loeb, *J. Cosmol. Astropart. Phys.* **06** (2021) 044.
- [44] S. Kawamura *et al.*, *Classical Quantum Gravity* **23**, S125 (2006).
- [45] G. M. Harry, P. Fritschel, D. A. Shaddock, W. Folkner, and E. S. Phinney, *Classical Quantum Gravity* **23**, 4887 (2006).
- [46] The z_s can even extend to 15 in our mocked samples, but when $z > 8$, the probability has become so small that can be ignored.
- [47] D. L. Jow, S. Foreman, U.-L. Pen, and W. Zhu, *Mon. Not. R. Astron. Soc.* **497**, 4956 (2020).
- [48] S. G. Murray, C. Power, and A. S. G. Robotham, *Astron. Comput.* **3**, 23 (2013).
- [49] L. S. Finn, *Phys. Rev. D* **53**, 2878 (1996).
- [50] Y. Zhao and Y. Lu, *Mon. Not. R. Astron. Soc.* **500**, 1421 (2021).
- [51] B. P. Abbott *et al.* (LIGO Scientific and Virgo Collaborations), *Astrophys. J. Lett.* **913**, L7 (2021).
- [52] J. Chen, C.-S. Yan, Y.-J. Lu, Y.-T. Zhao, and J.-Q. Ge, *Res. Astron. Astrophys.* **21**, 285 (2021).
- [53] K. Yagi and N. Seto, *Phys. Rev. D* **83**, 044011 (2011).